

# A Two-stage Single-phase Grid-connected Solar-PV System with Simplified Power Regulation

*Ganesh Moorthy Jagadeesan, Raja Pitchaimuthu\* and Moorthi Sridharan*

(Department of Electrical and Electronics Engineering,  
National Institute of Technology, Tiruchirappalli 620015, India)

**Abstract:** This study focuses on the design and development of a simplified active power regulation scheme for a two-stage single-phase grid-connected solar-PV (SPV) system with maximum power point (MPP) estimation. It aims to formulate and test an improvised new control scheme to estimate the real-time MPP of the PV panel and operate only at either the MPP or on the right-hand side (RHS) of the PV characteristics of the panel. A simple active power regulatory control scheme was formulated to provide frequency control services to a single-phase grid without using an energy storage device. The plant operator provides the reserve fraction as the input for the active power regulation controller. At any time, the reserve fraction is used to determine the magnitude of the reference power to be extracted from the PV panel for injection into the grid. A simple PI controller was used to track the calculated reference power. The different modes of operation of the regulatory scheme are presented in detail. All the above control schemes are integrated and implemented through appropriate switching of the DC-DC converter alone. The DC-AC converter maintains the DC link voltage and unity power factor at the single-phase grid terminals. The proposed control schemes were tested on a 250 Wp solar panel feeding power to a 230 V, 50 Hz single-phase grid through a two-stage converter. The entire scheme was modeled using the Matlab/Simulink platform, and the same was validated by hardware experimentation using Chroma Solar Simulator and NI myRIO controller under varied irradiation, temperature, and reserve fractions. The simulation and hardware results are compared and reported.

**Keywords:** Solar photo voltaic (SPV), maximum power point (MPP), right hand side (RHS), power regulation

## 1 Introduction

Currently, renewable energy sources have a significant role in replacing the usage of fossil fuels because of their environmental effects, such as global warming, air pollution, and various health hazards [1]. To effectively utilize renewable energy sources, such as solar photovoltaic and wind turbines, there is a need for efficient power control techniques under various operating condition [2-4]. Currently, grid-connected solar-PV power plants are preferably operated in the maximum power point (MPP) mode to maximize revenue. A direct real-time computation of MPP estimation techniques was proposed in Refs. [5-8]. The algorithm developed in Ref. [5] for MPP estimation has two loops of computation, which is overly complex. The use of a single-diode model SPV for MPP estimation,

with all the circuit parameters in Refs. [7-8], leads to an iterative-based estimation.

However, the method proposed in Ref. [9] neglects the effect of series and shunt resistances of the SPV model; thus, it avoids the conventional iteration-based estimation of the MPP. In turn, the controller reacts faster for dynamic changes in the reference conditions. Considering the shortcomings of Refs. [7-8], this study attempts to implement the analytical solution given in Ref. [9] to suit the grid-connected solar-PV system, in addition to the proposed enhanced active power regulation scheme.

Consequently, if the penetration level of the SPV is high, the MPPT mode can severely weaken the power system stability during grid disturbances. The stability of the power system can be improved by adopting an appropriate storage device along with its control. The installation of a storage system with renewable energy increases the cost and complexity of the control [10]. Hence, an appropriate method of active power

Manuscript received September 5, 2021; revised December 3, 2021; accepted January 31, 2022. Date of publication March 31, 2022; date of current version February 7, 2022.

\* Corresponding Author, E-mail: praja@nitt.edu  
Digital Object Identifier: 10.23919/CJEE.2022.000008

regulation in a grid-connected solar-PV system without any storage would make the system simple and cost effective<sup>[11]</sup>. Generally, active power control is achieved at the grid-tied inverter through various control schemes. A complex nonlinear adaptive backstepping controller is used. Similarly, in Ref. [12], active power regulation is achieved by phase-shifting the grid-connected inverter output voltage with respect to the grid voltage.

Further, in Refs. [13-16], attempts have been made to implement active power regulation in SPV systems at the DC-DC converter side. The advanced control techniques used in Refs. [13-14] can regulate the SPV output power according to any setpoint and force the SPV systems to operate on the left side of the MPP. However, power reference variation of near-zero to 100% of the available maximum power is impossible, and wide variation in power reference causes instability problems. The authors of Ref. [15] proposed a sensorless power reserve control strategy for two-stage grid-connected SPV systems using the FOCV-based MPPT technique. In Ref. [16], the DC-DC converter controls the active power curtailment with 10 PI controllers, and the system operates in the LHS of the SPV characteristics. The authors have not addressed a wide range of power references i.e., 0-100 %.

In this work, for the effective power reference variation of near-zero to 100% of the available maximum power, the proposed active power regulation scheme was designed to operate on the right-hand side of the PV characteristics of the PV system with minimal computational effort compared to Ref. [17]. To test the proposed active power regulation scheme, a two-stage grid-connected PV system, as shown in Fig. 1, is considered in the study. The proposed active power regulation scheme is mathematically modeled for a capacity of 250 Wp in Matlab/Simulink, and the same has been validated experimentally in the laboratory using Chroma Solar Simulator and NI myRIO controller for various operating conditions.

The uniqueness of the proposed scheme are as follows: ① A simplified active power regulation scheme for the DC-DC converter. As a result, the power reserve operation is achieved by controlling only one power electronic device; ② only one PI controller regulates the active power reference, rather

than conventional voltage control, ③ capability to regulate active power by operating at MPP, or to the RHS of MPP through an external reserve command under all environmental conditions. ④ Achieving the operation of the PV system in the RHS of PV characteristics through a simplified algorithm with a reduced computational burden. The RHS operation is valid irrespective of the MPP or power-regulation mode of operation. ⑤ The single-phase inverter performs DC link voltage control, grid synchronization, and UPF operations only.

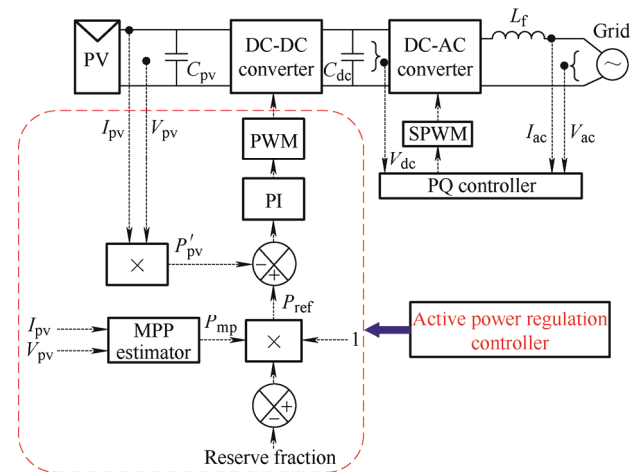


Fig. 1 Two-stage grid-connected single-phase solar-PV system with control logic

The proposed active power regulation scheme is described in Section 2 of this paper, and Section 3 explains the MPP estimation procedure. The solar-PV right-hand side operation for a two-stage grid-connected inverter combined with the power regulation operation is elaborated in Section 4. Sections 5 and 6 discuss the validation of the proposed control techniques using Matlab/Simulink and its hardware implementation. The concluding remarks are presented in Section 7.

## 2 Proposed active power regulation scheme

An important consideration for the power regulation control scheme is to provide a given amount of reserve, either in terms of absolute power (kW/MW) or as a fraction of the available maximum power represented as a reserve fraction. Hence, the control of the PV system was proposed in Ref. [3] to make it work as a conventional steam/hydro-driven grid-connected alternator. In conventional alternators, power

generation is based on customer demand by increasing hydro or steam input. Similarly, solar-PV-based power generation is expected to hold a controller function based on the external command given by the operator. This, in turn, aims to utilize the power corresponding to the operator requirement by estimating the maximum power. The specified reserve control can be achieved either by storing the excess energy or by maintaining the power reserve by injecting the specified power into the grid as a fraction of the estimated maximum power.

When active power regulation is in operation, most of the operating conditions cause the solar-PV to deliver power at a reduced level compared to the MPP, which leads to two possible operating points in the power vs. voltage characteristics of solar-PV. If the controller pushes the operating point to the left-hand side of the power vs. voltage characteristics, the following undesirable conditions will occur: (a) restriction on the operating range of the DC-DC converter, (b) increase in voltage and power ripples during transient operating conditions, and (c) restriction on power regulation from near-zero to maximum power ( $P_{mp}$ ). On the other hand, by overcoming the aforementioned disadvantages in left-hand side operation along with a decrement in losses can be achieved at the right-hand side operation, which operates at a lower current, thereby increasing the overall efficiency. The authors in Ref. [17] proposed a right-hand side operation, but as it requires graphical extrapolation and a Newton quadratic interpolation-based iterative process, the techniques are complex in terms of implementation in a digital controller. In this study, a simplified mechanism is used to bring the operating points to the right-hand side of the MPP under the power regulation mode.

Fig. 1 depicts a two-stage transformerless single-phase grid-connected solar-PV system with power processing stages of DC-DC and DC-AC conversions. The power injected to the grid is regulated by controlling the duty cycle of a 20 kHz DC-DC converter with required DC link voltage. The SPWM inverter performs the DC-link voltage control and also maintains the power quality and unity power factor at the grid end with a provision to support any ancillary service policy. From Fig. 1, the PI controller obtains the

error by comparing  $P'_{pv}$  and  $P_{ref}$ . The reference power to be injected,  $P_{ref}$ , is computed as in Eq. (1)

$$P_{ref} = P_{mp} \times (1 - \text{reserve fraction}) \quad (1)$$

where the reserve fraction is externally given by the grid operator based on the grid requirements. From the estimated MPP ( $P_{mp}$ ), reserve command, and the current operating point of the PV panel, such as  $V_{pv}$ ,  $I_{pv}$ , and  $P'_{pv}$ , the PI controller pushes the solar-PV operating point to the right-hand side of the power vs. voltage characteristics. The authors in Ref. [17] proposed active power control to obtain  $P'_{pv}$ , with 'if' and 'else' logic for making a decision based on  $V_{mp}$  and  $V_{pv}$ . Furthermore, interpolation techniques for the RHS operation of the MPP were used. In contrast, in the proposed method, the operating condition of  $P'_{pv}$  is directly compared with  $P_{ref}$  to make it operate on the right-hand side of the solar-PV characteristics under all environmental conditions with a specified reserve by verifying that the value of  $V_{pv}$  is greater than  $V_{mp}$ .

### 3 Estimation of maximum power point (MPP)

The essential mathematical expressions required for the real-time estimation of MPP are solar-PV voltage and current in terms of solar-PV equivalent circuit parameters. The connectivity between these parameters under reserve operating conditions is discussed in this section. This will help in the design of the controller for the DC-DC converter operation.

In general, the output current ( $I_{pv}$ ) of solar-PV with ' $n$ ' number of cells connected in series is given by Eq. (2)

$$I_{pv} = I_L - I_D [\exp((V_d / naV_t) - 1)] - (V_d / R_{sh}) \quad (2)$$

where  $a$  represents the diode quality factor,  $I_L$  is the light generated current of the module,  $I_D$  represents the dark current,  $V_t$  is the thermal voltage and  $V_d$  is the diode voltage, and  $R_{sh}$  is the parallel resistance of the module. As per Fig. 2, the diode voltage  $V_d$  can be written as

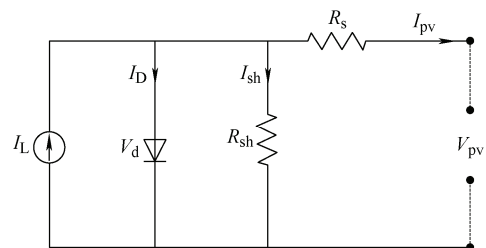


Fig. 2 Single-diode circuit model of a solar-PV cell

$$V_d = V_{pv} + I_{pv} R_s \quad (3)$$

where  $R_s$ ,  $V_{pv}$ , and  $I_{pv}$  are the series resistance, voltage, and current of the solar-PV module, respectively.

To implement real-time estimation of the MPP ( $P_{mp}$ ) by feeding the values of  $V_{pv}$  and  $I_{pv}$ , the values of Eqs. (7-8) are computed in the digital controller, as shown in Fig. 3. This gives the actual MPP at the corresponding irradiation and temperature. While computing the current and voltage corresponding to the MPP, the effects of  $R_{sh}$  and  $R_s$  are neglected to reduce the computational complexity. The current and voltage expressions are given by Eqs. (5-6) in Fig. 3. Further, for the inclusion of appropriate effects due to  $R_{sh}$  and  $R_s$ , the expressions of  $I_{mp}$  and  $V_{mp}$  (Eqs. (7-8)) have been proposed<sup>[9]</sup>.

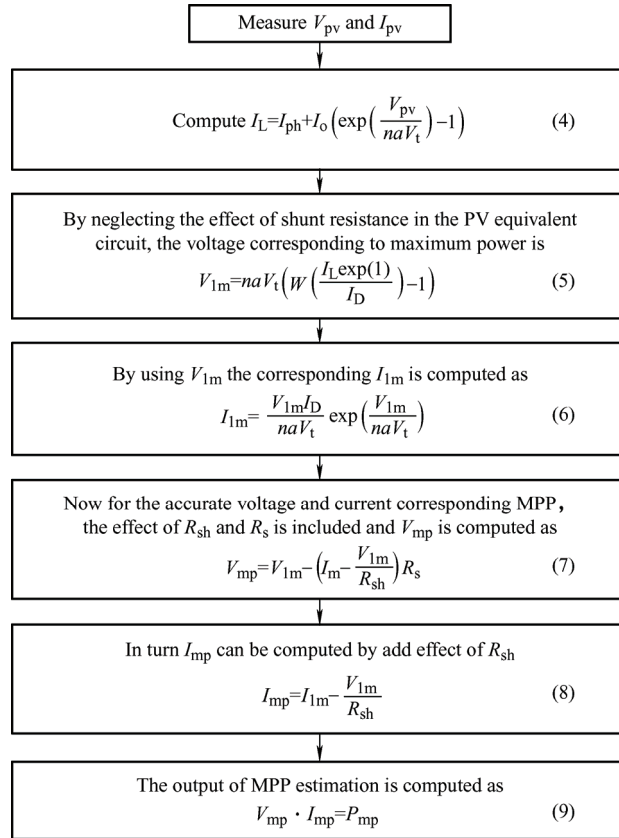


Fig. 3 MPP estimating procedure

For the above MPP estimating procedure, except for the measured values ( $V_{pv}$ ,  $I_{pv}$ ), the remaining values such as  $I_D$ ,  $I_0$ ,  $V_t$ ,  $n$ ,  $a$ ,  $R_s$ , and  $R_{sh}$  were obtained from the datasheets. Furthermore, owing to the degradation and aging of the PV array, these values may vary. To avoid errors in MPP estimation, periodic online

updating of these parameters is preferable.

#### 4 Solar-PV-RHS operation

While performing active power control in solar-PV, there are two possible operating points lying at either side of the MPP (LHS and RHS)<sup>[17]</sup> that favor operating at the RHS of PV characteristics where  $V_{pv}$  is greater than  $V_{mp}$ . This avoids the minimum voltage violation of the DC-DC converter at maximum reserve levels, has a faster dynamic response due to the slope at the RHS, and thus improves the efficiency of the converter. To obtain active power control<sup>[17]</sup>, an algorithm based on the Newton quadratic interpolation (NQI) method, which is an iterative process to obtain the required voltage of the PV array by approximating the PV characteristic curve with a quadratic curve, is proposed. The proposed work in this study intends to enable the RHS operation of a solar-PV system with a simplified control technique compared to Ref. [17]. As shown in Fig. 1, the RHS operation is obtained by directly comparing  $P'_{pv}$  and  $P_{ref}$ , which operate under all environmental conditions.

Tab. 1 is formulated by considering the environmental conditions and reserve requirements to estimate the present operating point of  $P'_{pv}$ . The following three cases were considered in the design and analysis of the controller.

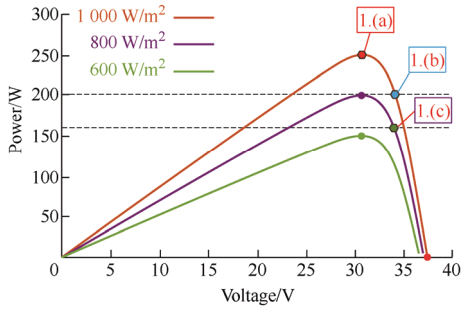
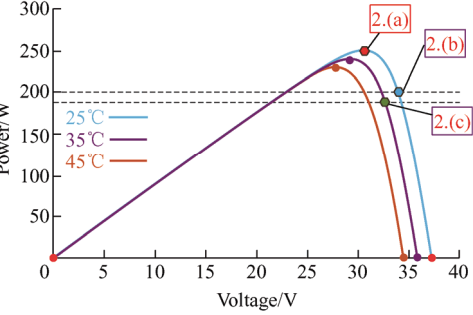
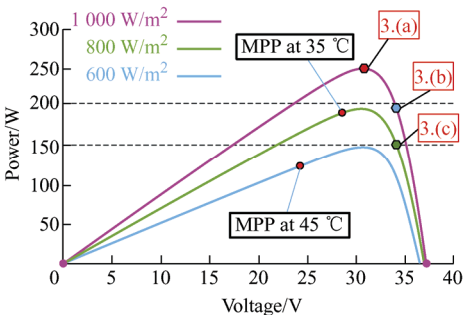
Case-1: Effect of variation in irradiation with the fixed temperature at 25 °C.

Case-2: Effect of temperature variation under fixed irradiation of 1 000 W/m<sup>2</sup>.

Case-3: Simultaneous variation in both irradiation and temperature.

For all the above cases of environmental variation, the possible changes in the reserve fraction are considered as subcases in the same table. This indicates the elimination of the complex mathematical techniques proposed in Ref. [17] for the RHS operation under specific conditions. The entire study helps in arriving at the conditions to be incorporated into the overall controller given in Fig. 1. Further, for clarity, all three cases are discussed in Tab. 1; Case-1 is elaborated in Fig. 4, and the rest of the cases are self-explanatory, as shown in Figs. 5 and 6 of Tab. 1.

**Tab. 1 Various operating cases proposed under active power reserve control**

PV characteristics under various operating conditions	References values	Power constraint	Operating voltage
<p>Case-1</p>  <p>Fig. 4 Variation in irradiation under 25 °C</p>	<p>1.(a) Reserve=0; <math>P_{ref}=P_{mp}</math></p> <p>1.(b) Reserve=<math>\chi&gt;0</math>; <math>P_{ref}=(1-\chi)P_{mp}</math></p> <p>1.(c) Reserve is retained as in condition 1.(b)</p>	<p><math>P'_{pv}=P_{mp}</math></p> <p><math>(P'_{pv})_b &lt; P_{mp}</math></p> <p><math>(P'_{pv})_c &lt; (P_{mp})_a</math></p>	<p><math>V_{pv}=V_{mp}</math></p> <p><math>(V_{pv})_b &gt; (V_{mp})_a</math></p> <p><math>(V_{pv})_c \geq (V_{mp})_a</math></p>
<p>Case-2</p>  <p>Fig. 5 Variation in temperature under 1000 W/m<sup>2</sup></p>	<p>2.(a) Reserve=0; <math>P_{ref}=P_{mp}</math></p> <p>2.(b) Reserve=<math>\chi&gt;0</math>; <math>P_{ref}=(1-\chi)P_{mp}</math></p> <p>2.(c) Reserve is retained as in condition 2.(b)</p>	<p><math>P'_{pv}=P_{mp}</math></p> <p><math>(P'_{pv})_b &lt; P_{mp}</math></p> <p><math>(P'_{pv})_c &lt; (P_{mp})_a</math></p>	<p><math>V_{pv}=V_{mp}</math></p> <p><math>(V_{pv})_b &gt; (V_{mp})_a</math></p> <p><math>(V_{pv})_c \geq (V_{mp})_a</math></p>
<p>Case-3</p>  <p>Fig. 6 Variation in both irradiation and temperature</p>	<p>3.(a) Reserve=0; <math>P_{ref}=P_{mp}</math></p> <p>3.(b) Reserve=<math>\chi&gt;0</math>; <math>P_{ref}=(1-\chi)P_{mp}</math></p> <p>3.(c) Reserve is retained as in condition 3.(b)</p>	<p><math>P'_{pv}=P_{mp}</math></p> <p><math>(P'_{pv})_b &lt; P_{mp}</math></p> <p><math>(P'_{pv})_c &lt; (P_{mp})_a</math></p>	<p><math>V_{pv}=V_{mp}</math></p> <p><math>(V_{pv})_b &gt; (V_{mp})_a</math></p> <p><math>(V_{pv})_c \geq (V_{mp})_a</math></p>

Case-1: Effect of variation in irradiation with the fixed temperature at 25 °C.

In all the instances of the PV characteristics during Case-1, (shown in Fig. 4), if the reserve fraction is assigned as ‘zero’, the DC-DC converter is forced to deliver the maximum power. Hence,  $P'_{pv}$  will be equated to  $P_{mp}$  and, in turn,  $V_{pv}$  should be equal to  $V_{mp}$ , as shown in 1.(a) of Fig. 4. For the positive fractional input reserve fraction with the same irradiation,  $(P_{ref})_b$

will become less than  $(P'_{pv})_a$  at the MPP, and this error will be reduced to zero by the PI controller by making  $(V_{pv})_b$  greater than  $V_{mp}$ , which leads to right-hand side operation in the solar-PV characteristics (shown in 1.(b) of Fig. 4). At 1.(c) in Fig. 4, if the reserve fraction is retained, as in instance 1.(b), and the irradiation is reduced, then  $(P'_{pv})_c$  will appear at the comparator, which is less than  $(P_{ref})_b$ ; hence,  $V_{pv}$  will be adjusted accordingly to maintain the RHS operation.

## 5 Simulation studies

The overall block diagram shown in Fig. 1 is modeled using Matlab/Simulink to investigate the performance of the proposed MPP estimator and controller for the right-hand side operation of a 250 Wp solar-PV system. The major system parameters considered for this simulation study are listed in Tabs. 2 and 3. To validate the effectiveness of the proposed technique, the three cases listed in Tab. 1 were simulated, and their corresponding results are presented in this section.

**Tab. 2 PV module parameters**

Parameter	Actual value
Open circuit voltage $V_{oc}/V$	37.3
Short circuit current $I_{sc}/A$	8.66
Maximum voltage $V_m/V$	30.7
Maximum current $I_m/A$	8.15
Maximum power $P_m/Wp$	250.205
Series resistance $R_s/\Omega$	0.237 2
Shunt resistance $R_{sh}/\Omega$	224.18
Diode quality factor $a$	1.019

**Tab. 3 PV module parameters**

Parameter	Actual value (in SI units)
Switching frequency $f_s/kHz$	20
Input capacitance $C_{pv}/\mu F$	2
DC link capacitance $C_d/\mu F$	450
Inductance $L/mH$	20
PI controller $K_p$	0.15
PI controller $K_i$	5

First, the transient response of the controller is tested under various environmental conditions, such as irradiation and temperature. The grid-injected real power under various irradiances was simulated under a fixed panel temperature of 25 °C with zero reserve fraction. The proposed technique tracked the estimated maximum power corresponding to the irradiation, and the same power was injected into the AC grid through the inverter, as depicted in Fig. 7. The variation of the MPP and grid injected power with respect to irradiation and zero reserve fraction under a change in temperature are plotted in Fig. 8. In these cases, the tracking of the controller is sufficiently fast to

compute the MPP and deliver the same to the grid.

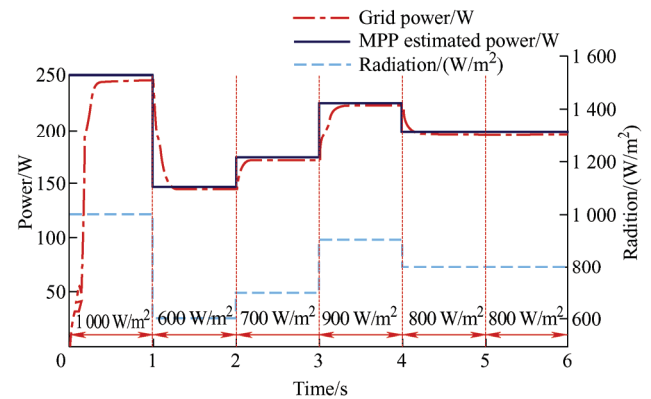


Fig. 7 Variation in maximum power estimation and grid power under various irradiation at 25 °C with zero reserve

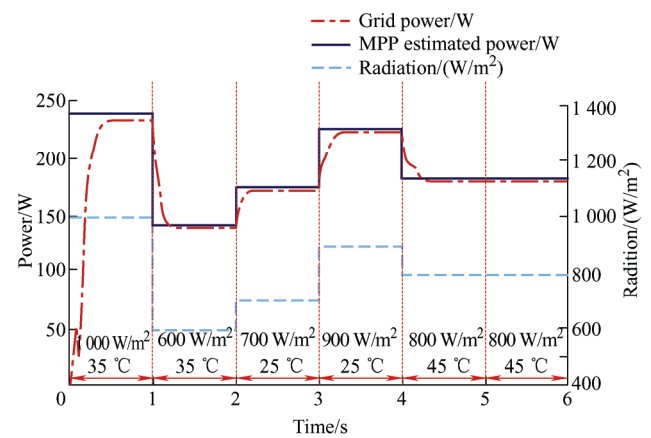


Fig. 8 Variation in maximum power estimation and grid power under varied irradiation and temperature with zero reserve

From Fig. 9, the difference between the MPP and grid-injected power is evident owing to the reserve operation. To validate the above claim, the power in the instances of 0.5 s and 1.5 s in Fig. 9 are analyzed. At 0.5 s, the grid power to be injected is 200 W, whereas the estimated MPP power is 250 W; hence, the reserve fraction is set as 0.2 to bring down the MPP power and equalize it to the required grid power. Similarly, at 1.5 s, the estimated MPP power is 150 W, which is equal to the grid power to be injected. Hence, the reserve fraction is set as 'zero' to feed the grid with a power of 150 W.

To demonstrate the effect of simultaneous changes in parameters such as irradiation, temperature, and the reserve ratio, the simulation is carried out for various values, and the same is plotted in Fig. 10. It can be seen from the figure that the dynamic changes in all



the parameters are considered while designing the control scheme and the above-mentioned parameters.

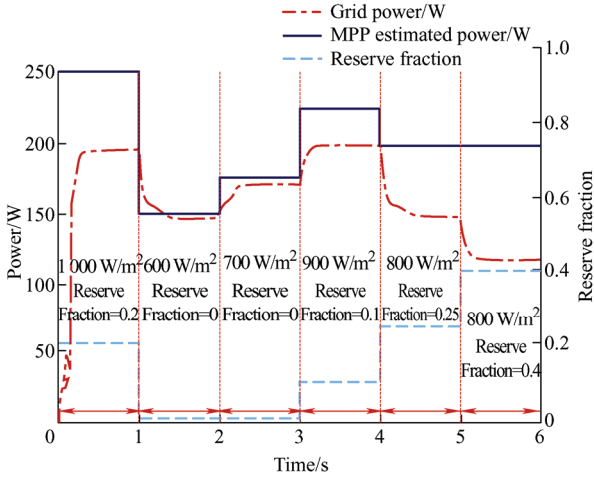


Fig. 9 Variation in maximum power estimation and grid power under varied irradiation at constant temperature 25 °C with reserve fraction

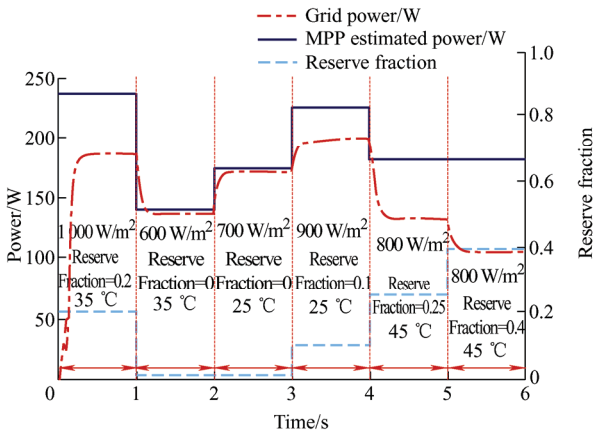


Fig. 10 Variation in maximum power estimation and grid power under varied irradiation and temperature with the change in reserve fraction

To validate the RHS operation under various operating conditions, the power versus voltage characteristics are plotted with the corresponding RHS and LHS points in Fig. 11. The difference in the change in operating voltage with respect to the shift in  $P'_{pv}$  for the change in reserve fraction is minimal when the shift occurs in the RHS compared to the LHS. These operations reduce the voltage stress on the DC-DC converter and help improve the settling time of the overall controller. From Tab. 1, the relationship between  $V_{mp}$  and  $V_{pv}$  should be verified to ensure the RHS operation under all possible environmental conditions.  $V_{mp}$  being less than  $V_{pv}$  confers the RHS operation under specific operating conditions. For this

purpose, the variation of both voltages was plotted by varying the irradiation and temperature, which confirmed that for all the combinations of the operating parameters (irradiation, temperature, and reserve fraction),  $V_{pv}$  is higher than  $V_{mp}$ , as shown in Fig. 12.

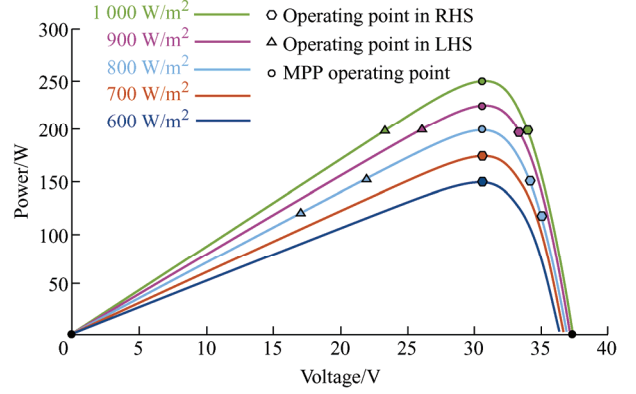


Fig. 11 Operating power points of solar-PV under varied irradiation and reserve fraction

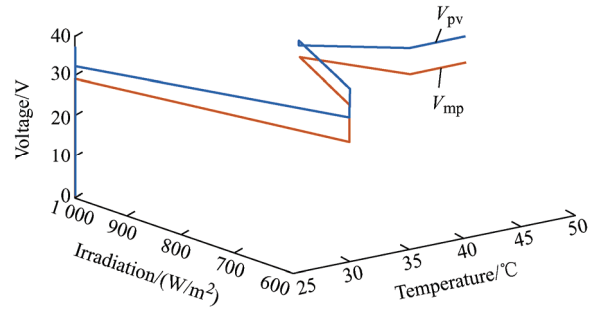


Fig. 12 Comparison of MPP( $V_{mp}$ ) and solar-PV( $V_{pv}$ ) voltage with respect to irradiation and temperature

Tab. 4 enumerates the duty cycle validation during various irradiation and reserve fractions. It can be observed that whenever the reserve fraction is given by the grid operator, the designed PI controller regulates the power ( $P_{pv}$ ) from the estimated power ( $P_{mp}$ ) for any particular irradiation and temperature. Hence,  $P_{pv}$  decreases as the corresponding duty cycle increases. It is observed and validated that  $V_{pv}$  operates in the RHS of PV characteristics during reserve fraction ( $R_{es}$ ).

Tab. 4 Duty cycle validation during reserve operation

Irradiation/ (W/m <sup>2</sup> )	Temp./°C	Res. (%)	$P_{mp}$ /W	$P_{pv}$ /W	Duty cycle
1 000	25	0	250	250	0.90
1 000	25	0.20	250	250	0.94
800	25	0	200	200	0.86
800	25	0.25	200	150	0.91

Fig. 13 depicts the  $V_{mp}$  and  $V_{pv}$  values for reserve fractions between 0 and 4 %. When the reserve fraction is zero,  $V_{mp}$  becomes equal to  $V_{pv}$ . It is observed that whenever there is an increase in the reserve fraction, the corresponding  $V_{pv}$  values also increase. This observation validates the effectiveness of the proposed active power regulation without the involvement of any complex mathematical operation and implementation compared to the methods in the literature.

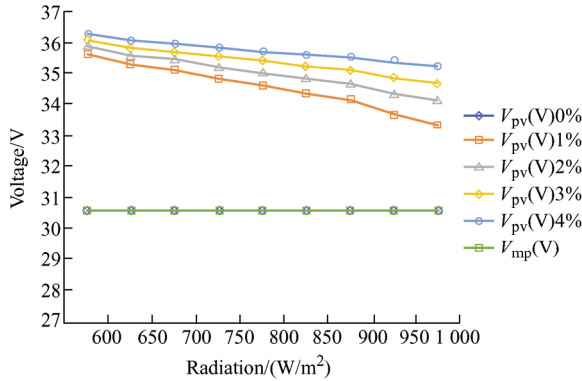


Fig. 13  $V_{mp}$  and  $V_{pv}$  for various radiation and reserve fractions

The proposed method of MPP estimation and the traditional MPPT method of P&O are compared here with respect to ripple content in the SPV output power ( $P_{pv}$ ) and voltage ( $V_{pv}$ ) in Figs. 14. and 15, respectively. The obtained results show that the ripples in  $P_{pv}$  and  $V_{pv}$  are marginally reduced in the MPP estimation method.

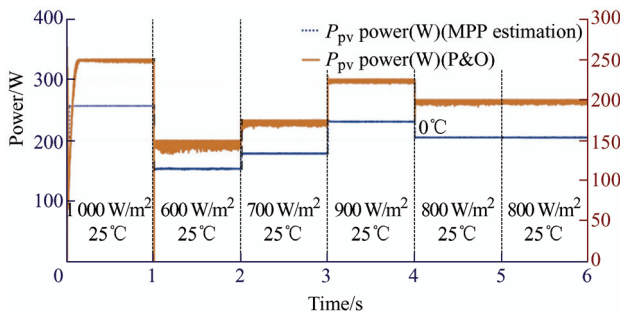


Fig. 14 Comparison between MPP estimation and P&O for  $P_{pv}$  power ripple

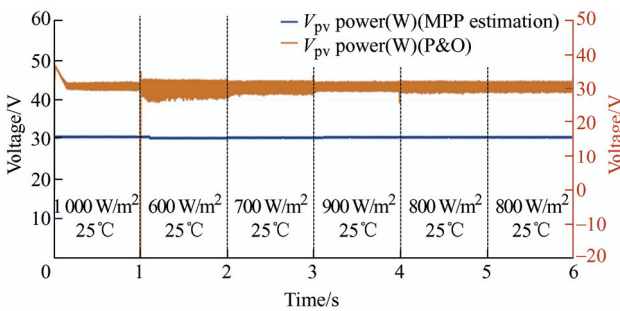


Fig. 15 Comparison between MPP estimation and P&O for  $V_{pv}$  ripple

The experimental results of the proposed algorithm with the real solar-PV panels are shown in Figs. 16 and 17. It is observed that the experimental results obtained for the available irradiances of 615 W/m<sup>2</sup> and 725 W/m<sup>2</sup> with panel temperature and reserve fraction are in close correspondence with the simulated results for the same conditions.

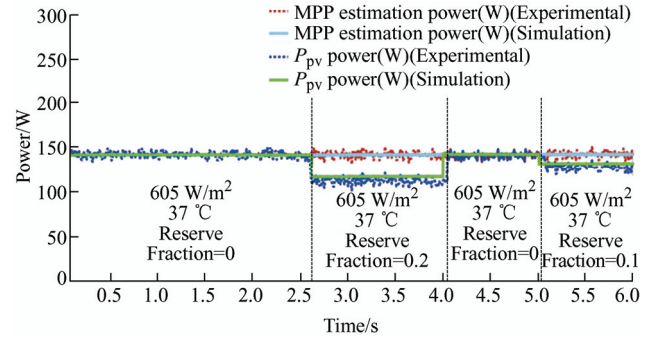


Fig. 16 Change in SPV power ( $P_{pv}$ ) under varied operating conditions (605 W/m<sup>2</sup>)

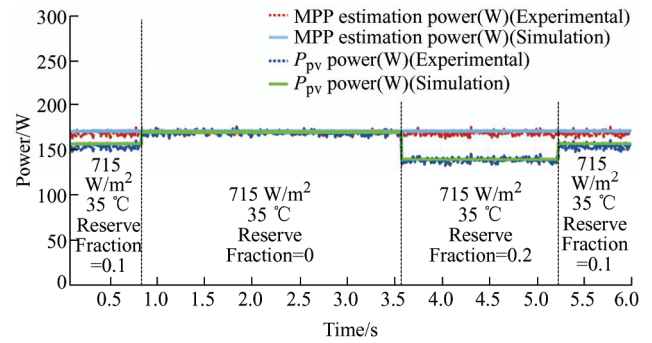


Fig. 17 Change in SPV power ( $P_{pv}$ ) under varied operating conditions (715 W/m<sup>2</sup>)

The performance of the DC-AC converter with the associated PQ controller is validated by plotting the change in the grid current with respect to time, as shown in Fig. 18. The grid injected current at zero reserves (for conditions mentioned in Fig. 8) and with different non-zero reserve fractions (for conditions mentioned in Fig. 10) are compared and depicted in Fig. 18. Because the grid voltage is kept constant, the trace of change in the grid current is very well seen with respect to the change in irradiation, temperature, and reserve fraction.

Whenever a grid-tied inverter is implemented, it is essential to study the quality of the current injected into the grid in terms of shape and total harmonic distortion (THD). The current waveform is shown in Fig. 19, and the corresponding frequency spectrum with a THD of 2.32 %, as shown in Fig. 20, validates the design of the power quality controller and filter. In Fig. 19, the injected grid current is in phase with the



grid voltage, which confirms the zero reactive power at the grid terminals.

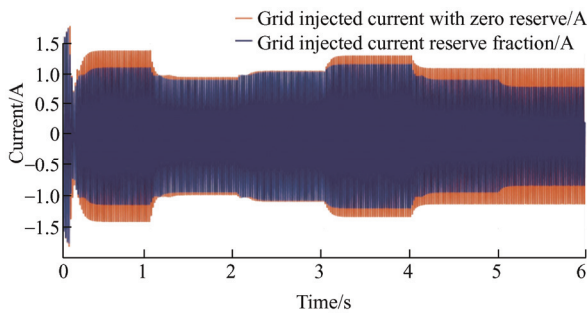


Fig. 18 Grid injected current corresponding to the various irradiation, temperature, and reserve fraction

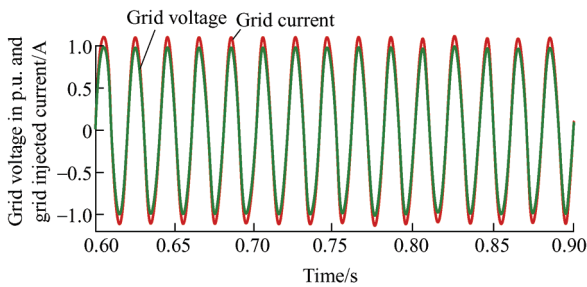


Fig. 19 Grid voltage in p.u. and grid injected current

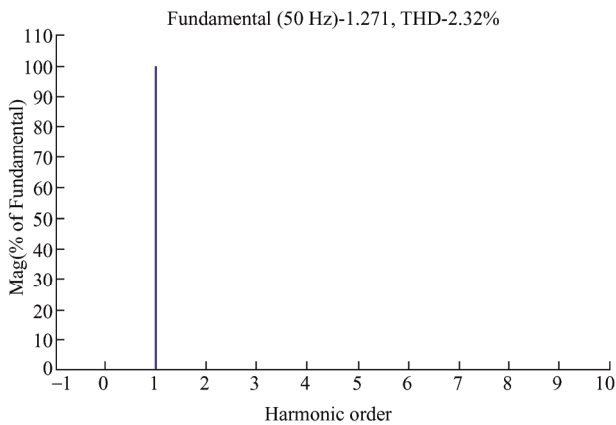


Fig. 20 THD in grid current

The simulation results reported above (From Figs. 7-20) were validated with the help of hardware experimentation in the forthcoming section.

## 6 Experimental studies

Fig. 21 depicts the two-stage single-phase grid-connected solar-PV inverter in which a Chroma-make solar simulator of 250 Wp is used instead of a solar panel. The proposed MPP estimation and essential control were programmed in an NI-myRIO digital controller. The variation of irradiation and temperature is given as inputs to the solar simulator, and the reserve fraction is given through the NI-myRIO

controller. The dynamic variations in the MPP-estimated data and PV actual output data were stored in the NI-myRIO data logger and plotted using Matlab. The grid-side parameters such as grid voltage, current, real power, reactive power, and power factor were captured using a Fluke-make single-phase power quality analyzer.

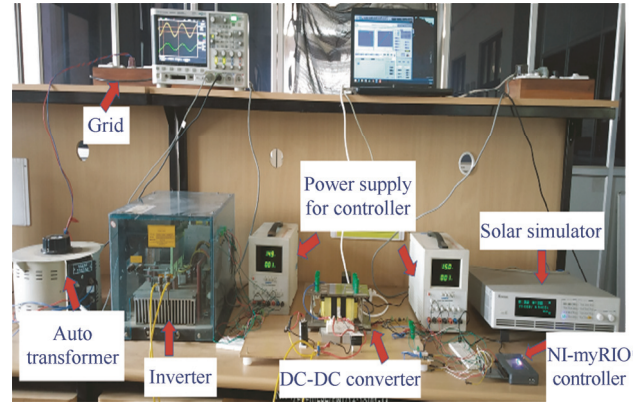


Fig. 21 Experimental setup for a two-stage single-phase grid-connected Solar-PV system

The MPP estimated power computed through simulation and inferred in the hardware under varied irradiation for a given temperature is plotted in Fig. 22. Fig. 23 shows the variation of grid power with respect to irradiation under a constant temperature of 25 °C captured in the simulation as well as in the hardware. Because the reserve fraction in both cases is considered to be zero, for all irradiancies, the MPP estimated power should be equal to the grid power, as shown in Figs. 22 and 23. It is observed that both simulation and hardware results closely match, which validates the effectiveness of the proposed techniques.

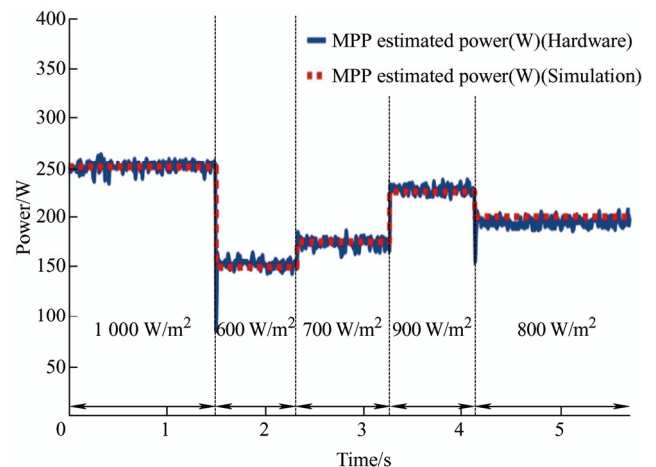


Fig. 22 Comparison of simulation and hardware results for variation in maximum power estimation under various irradiation at 25 °C with zero reserve fraction

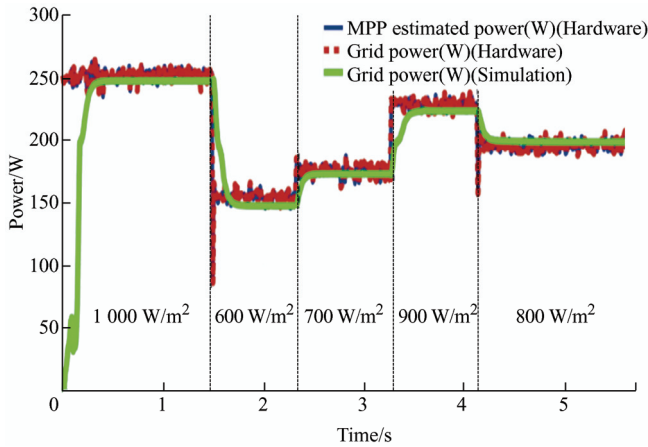


Fig. 23 Comparison of hardware and simulation results for grid power under varied irradiation and MPP estimation power with zero reserve fraction

As shown in Fig. 24, the grid power computed in the simulation and experimental setup was compared. They vary according to the given operating conditions, such as irradiation, temperature, and reserve fraction. The reserve power is the difference between the MPP-estimated power and the actual grid power, as shown in Fig. 24. The response time of the experimental setup for the change in the reserve fraction was very close to the response in the simulation. This validates the effective design of the hardware circuit and the speed of the controller for dynamic changes in the operating parameters.

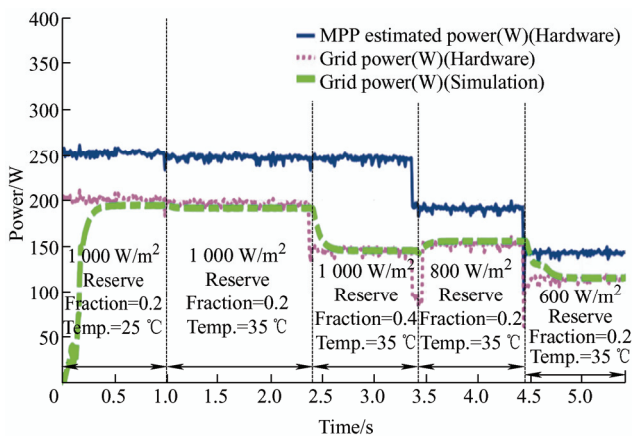
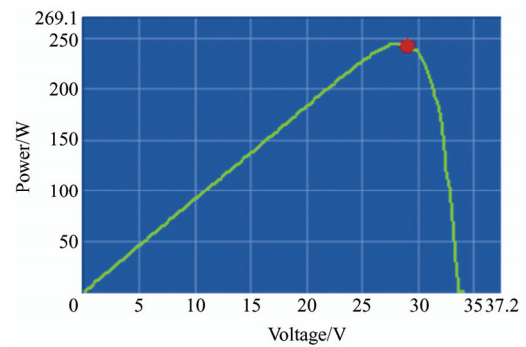


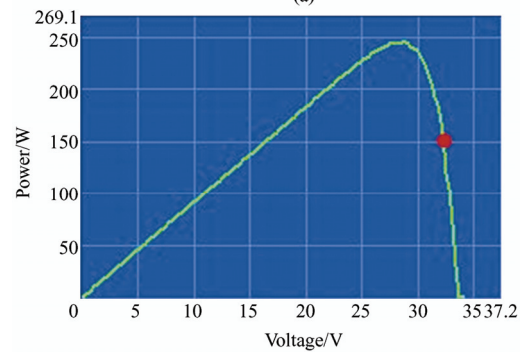
Fig. 24 Results of grid power and estimated MPP power under varied irradiation and temperature with the change in reserve fraction

The right-hand side operation of the solar-PV in its power characteristics has been claimed as a desirable operation under non-zero reserve conditions. To validate the same in the proposed power control algorithm, the power characteristics with the operating

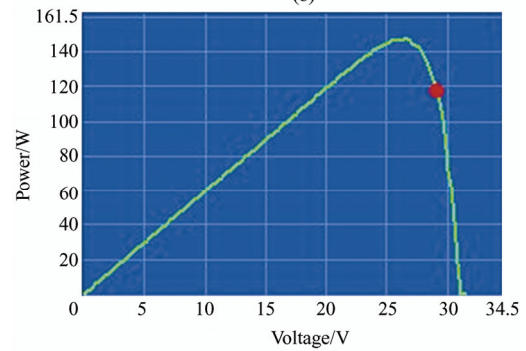
point inferred through the solar simulator display were used. In Fig. 25, it is shown that the operating points are shifted from the MPP to the right-hand side when a nonzero reserve fraction is introduced. Fig. 25a depicts the operating point at which the grid power equals the MPP estimated power at ‘zero’ reserve. Figs. 25b and 25c prove that the operating point in the PV characteristics is on the right-hand side for irradiation of 1 000 W/m<sup>2</sup> and 600 W/m<sup>2</sup> with reserve fractions of 0.4 and 0.2, respectively. The same temperature (35 °C) was maintained for all three operating conditions, as shown in Figs. 25a-25c.



(a)



(b)



(c)

Fig. 25 Solar-PV operating point under varied irradiation and temperature with the change in reserve fraction

The dynamic variations in the solar-PV voltage and current corresponding to the given changes in operating conditions are shown in Fig. 26. This figure reveals the right-hand side operating point in the PV

characteristics, which is inferred by an increase in voltage while the reserve fraction is introduced.

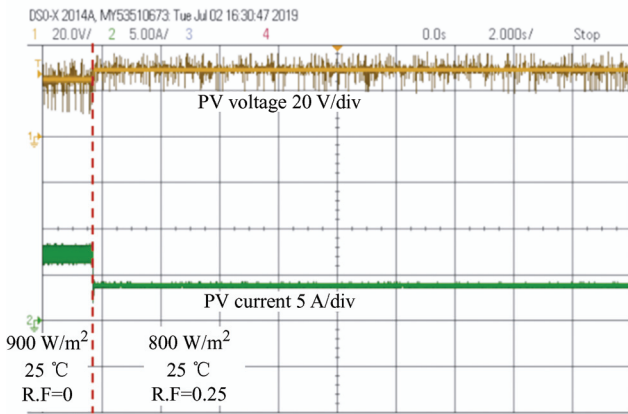


Fig. 26 PV output voltage and current under varied irradiation and reserve fraction

In Figs. 27 and 28, the parameters related to the grid are elucidated using a single-phase power quality analyzer to understand the impact of the proposed algorithm implemented in the experimental prototype. The particular recording is carried out by keeping 1 000 W/m<sup>2</sup>, 25 °C with ‘zero’ reserve, and it is noticed that the DC-AC converter offers a power factor near unity. Furthermore, the grid current is almost free from harmonics and is within the standard requirement.

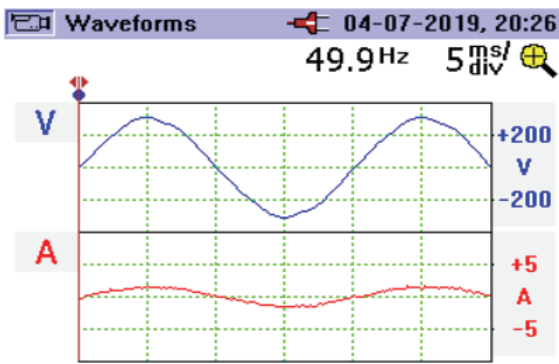


Fig. 27 Grid voltage and current

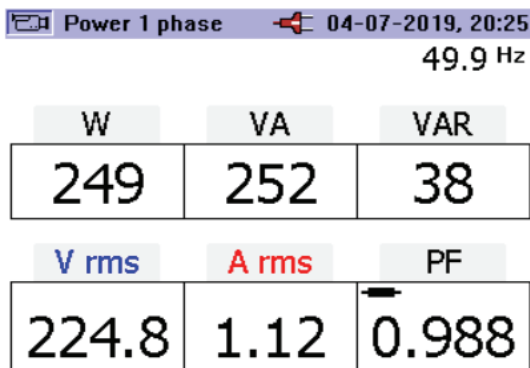


Fig. 28 Grid voltage, current, real, apparent, reactive power, and power factor

## 7 Conclusions

The proposed simplified active power control with reserve fraction over the entire operating range from near-zero to 100 % of the available MPP was tested and reported for various operating conditions. The RHS operating point of the SPV was maintained under all operating conditions with a specified reserve fraction. This was validated by observing the operating voltage of the SPV, along with the results obtained through the solar simulator. Further, the power quality was ensured at the grid terminals in the proposed scheme by maintaining the THD and zero reactive power exchange. The essential findings and results required for supporting the proposed scheme were provided by modeling and simulating a grid-connected 250 Wp solar-PV system. Subsequently, experimental results obtained by implementing a prototype setup with the same specifications in the laboratory helped to validate the effectiveness of the proposed active power regulation scheme.

## References

- [1] N Gelsora, N Gelsorb, T Wangmob, et al. Solar energy on the Tibetan plateau: Atmospheric influences. *Solar Energy*, 2018, 173: 984-992.
- [2] E Lorenzani, G Migliazza, F Immovilli, et al. CSI and CSI7 current source inverters for modular transformerless PV inverters. *Chinese Journal of Electrical Engineering*, 2019, 5(2): 32-42.
- [3] X Zhang, Q Gao, Y Hu, et al. Active power reserve photovoltaic virtual synchronization control technology. *Chinese Journal of Electrical Engineering*, 2020, 6(2): 1-6.
- [4] F Zhang, D Jiang, K Xu, et al. Two-stage transformerless dual-buck PV grid-connected inverters with high efficiency. *Chinese Journal of Electrical Engineering*, 2018, 4(2): 36-42.
- [5] E I Batzelis, S A Papathanassiou. A method for the analytical extraction of the single-diode PV model parameters. *IEEE Trans. Sustain. Energy*, 2016, 7(2): 504-512.
- [6] E I Batzelis, G E Kampitsis, S A Papathanassiou, et al. Direct MPP calculation in terms of the single-diode PV model parameters. *IEEE Trans. Energy Convers.*, 2015, 30(1): 226-236.
- [7] J S C M Raj, E Jeyakumar. A two-stage successive estimation based maximum power point tracking technique for photovoltaic modules. *Solar Energy*, 2014: 43-61.

- [8] S Wang, Q Chen, W Gao. An improved analytical solution for MPP parameters of photovoltaic cells. *Solar Energy*, 2018, 174(1): 848-854.
- [9] G Farivar, B Asaei, S Mehrnami. An analytical solution for tracking photovoltaic module MPP. *IEEE J. Photovoltaics*, 2013: 1053-1061.
- [10] H Yatimi, E Aroudam. Assessment and control of a photovoltaic energy storage system based on the robust sliding mode MPPT controller. *Solar Energy*, 2016, 139: 557-568.
- [11] T K Roy, M A Mahmud. Active power control of three-phase grid-connected solar-PV systems using a robust nonlinear adaptive backstepping approach. *Solar Energy*, 2017, 153: 64-76.
- [12] L Hassaine, E Olias, J Quintero, et al. Power control for grid-connected applications based on the phase shifting of the inverter output voltage with respect to the grid voltage. *International Journal of Electrical Power & Energy Systems*, 2014, 57: 250-260.
- [13] A Sangwongwanich, Y Yang, F Blaabjerg. A cost-effective power ramp-rate control strategy for single-phase two-stage grid-connected photovoltaic systems. *IEEE Energy Conversion Congress and Exposition (ECCE)*, Milwaukee, WI, 2016: 1-7.
- [14] A Sangwongwanich, Y Yang, F Blaabjerg. High-performance constant power generation in grid-connected PV systems. *IEEE Transactions on Power Electronics*, 2016, 31(3): 1822-1825.
- [15] A Sangwongwanich, Y Yang, F Blaabjerg. A sensorless power reserve control strategy for two-stage grid-connected PV systems. *IEEE Transactions on Power Electronics*, 2017, 32(11): 8559-8569.
- [16] A M Howlader, S Sadoyama, L R Roose, et al. Active power control to mitigate voltage and frequency deviations for the smart grid using smart PV inverters. *Applied Energy*, 2020, 258: 114000.
- [17] E Batzelis, G Kampitsis, S Papathanassiou. Power reserves control for PV systems with real-time MPP estimation via curve fitting. *IEEE Transactions on Sustainable Energy*, 2017, 8(3): 1269 -1280.



**Ganesh Moorthy Jagadeesan** received his B.E. degree in Electrical Engineering from Saranathan college of Engineering, Trichy and M.E. degree in Solar Energy from College of Engineering, Guindy, Chennai, and He is currently working towards his Ph.D at the solar photovoltaic converter topologies and grid connected PV systems at National Institute of

Technology, Tiruchurappalli, India.



**Raja Pitchaimuthu** obtained his M.Tech. degree in Energy Systems from Indian Institute of Technology Madras, Chennai in 2002 and Ph.D. degree from National Institute of Technology, Tiruchirappalli in 2013. He is presently an Associate Professor in the Department of Electrical and Electronics Engineering at National Institute of Technology, Tiruchirappalli at India

where he has been since 2006. His field of interest is design and development of controllers for power converters used in solar and wind energy conversion systems. He also does research in the development of protection schemes for transmission and distribution systems. He is a Senior Member in IEEE, Life Member of ISTE and Institution of Engineers (India).



**Moorthi Sridharan** is a faculty in the Department of Electrical and Electronics Engineering, National Institute of Technology, Trichy, India, since 2007 and is associated with the VLSI Systems Research Laboratory in the same department. He completed his Ph.D in the area of VLSI for Communication Circuits during 2008 at Anna University, Chennai. Further, he is a

Post-Doctoral fellow of Erasmus Mundus External Co-operation Window initiated under EURINDIA Programme in which he has done Post-Doctoral research on Memory Design for Reconfigurable Architectures at Royal Institute of Technology (KTH), Sweden. His research interests include VLSI for signal processing and embedded systems.